Hutt City Probabilistic Tsunami Hazard Maps

DR Burbidge
WL Power
AR Gusman
X Wang

GNS Science Consultancy Report 2021/115
November 2021

DISCLAIMER

This report has been prepared by the Institute of Geological and Nuclear Sciences Limited (GNS Science) exclusively for and under contract to Hutt City Council. Unless otherwise agreed in writing by GNS Science, GNS Science accepts no responsibility for any use of or reliance on any contents of this report by any person other than Hutt City Council and shall not be liable to any person other than Hutt City Council, on any ground, for any loss, damage or expense arising from such use or reliance.

Use of Data:

Date that GNS Science can use associated data: December 2021

BIBLIOGRAPHIC REFERENCE

Burbidge DR, Gusman AR, Power WL, Wang X. 2021. Hutt City Probabilistic Tsunami Hazard Maps. Lower Hutt (NZ): GNS Science. 26 p. Consultancy Report 2021/115.

CONTENTS

FIGURES

TABLES

EXECUTIVE SUMMARY

In 2021, Hutt City Council (HCC) contracted GNS Science to provide probabilistic tsunami inundation hazards maps to inform their District Plan. They requested that GNS Science produce probabilistic tsunami inundation maps for three annual probabilities of exceedance (APoEs), 1:100, 1:500 and 1:1000 years, and to then calculate the resulting inundation they cause at two different sea levels, present-day Mean High Water Springs (MHWS) and present-day MHWS plus 1.0 m of sea-level rise. To produce these maps, GNS Science used the latest update to their National Tsunami Hazard Model (NTHM) to select scenarios appropriate for each APoE for the zone offshore the Wellington region (Tsunami Hazard Zone 91). For all of the APoEs investigated here, the Hikurangi Subduction Zone contributed most of the hazard to this coastal zone. At the 1:100-year APoE, most of the hazard comes from a moment magnitude (M_W) 8.1 megathrust earthquake on this subduction zone, rising to a M_W 8.7 megathrust earthquake at the 1:1000-year APoE. For the 1:100-year APoE, most of the rest of the hazard comes from regional and distant subduction zones, such as Peru. However, at the 1:1000-year APoE, most of the rest of the hazard comes from large (M_W 7.9–8.4) magnitude earthquakes on local crust faults with a fault section lying offshore New Zealand (such as the offshore part of the Wairarapa Fault). These scenarios are the same as those used for a similar study recently completed for Wellington City Council (WCC) by Burbidge et al. (2021). GNS Science then used the grid originally developed for the WCC study and the scenarios described above to calculate the inundation expected from these scenarios in the region covered by HCC. Inundation models were run at two sea-level rise assumptions requested by HCC, and these were then combined using a weighted median approach to create probabilistic tsunami inundation maps for each APoE and sea-level rise combination. As expected, at the 1:100-year APoE, the extent of inundation is small at the current MHWS. However, at the 1:1000-year APoE, the inundation extents are much larger, with most of the inundation occurring in Petone, Seaview, Point Howard, Lowry Bay, York Bay, Mahina Bay, Days Bay and Eastbourne. Broadly speaking, increasing the MHWS by 1.0 m increases the probability of a given extent of inundation. For example, the inundation extent of the 1:100-year hazard map with an additional 1.0 m of sea-level rise is slightly larger than the extent of the 1:500-year hazard map without the extra metre of sea-level rise, although there are some differences in specific areas, mainly due to the different tsunami sources used at each APoE.

This page left intentionally blank.

1.0 INTRODUCTION

Hutt City Council (HCC) is currently undertaking a review of their District Plan (called 'the Plan' hereafter), including an assessment of the natural hazards potentially faced by the city. To help provide some underpinning science advice to inform the plan, HCC contracted GNS Science to provide probabilistic tsunami inundation hazards maps for the region covered by HCC. The maps need to cover three different annual probabilities of exceedance (APoE), 1:100, 1:500 and 1:1000 years, and two different sea-level assumptions; the present-day Mean High Water Springs (MHWS) and the present-day MHWS plus 1.0 m of sea-level rise.

The maps will need to include both the extents and depths of inundation (i.e. flow depths) at these APoEs and sea-level assumptions. For a visual explanation of terms such as 'flow depth', see Figure 3.1. The maps are to be accompanied by a methodology report (this document). The methodology used to produce the maps is based on that used in a previous study completed for Porirua City Council (PCC), funded by EQC (the Earthquake Commission) and PCC (Gusman et al. 2019a) and further developed in a study to provide similar probabilistic tsunami inundation maps for Wellington City Council (Burbidge et al. 2021) for their District Plan. This study covers as much of the urban area in HCC's jurisdiction as possible within Tsunami Hazard Zone 91 (Figure 1.1), limited to where there is adequate data.

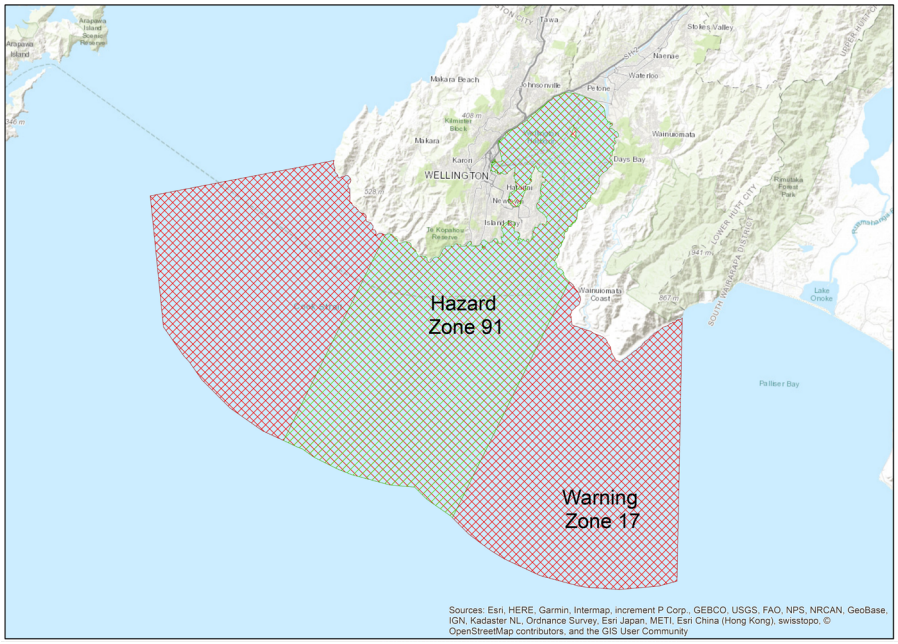

Figure 1.1 Tsunami coastal zones offshore of the Wellington region. This project is limited to the HCC jurisdiction in Tsunami Hazard Zone 91, which falls within Tsunami Warning Zone 17.

To help ensure that these maps are as robust as possible, we modelled the tsunami inundation coming from a range of different earthquake sources at each of the three APoE periods and two sea-level values, similar to the choices in Gusman et al. (2019a). The sources were selected based on the latest version of the National Tsunami Hazard Model (NTHM), which is currently being updated at the time of writing. The earthquake sources are identical to those in Burbidge et al. (2021), as both HCC and WCC lie within the same Hazard Zone and have requested the same APoEs. This also allows for some consistency between the plans developed by WCC and HCC.

The project was structured into three stages.

1.1 Stage 1: Scenario Selection

As stated above, GNS Science is currently updating the NTHM. This model has been used to deaggregate the hazard for Tsunami Hazard Zone 91, which has a length of approximately 20 km and is within Tsunami Warning Zone 17 (see Figure 1.1). From the deaggregation, we then selected the top six scenarios to represent the hazard to Zone 91 at the three different APoEs. This is the same as was done in Burbidge et al. (2021) for the WCC project. However, we repeat both the method and descriptions of the resulting scenarios in this report as well to help ensure that this is a 'stand-alone' report. This is done in Section 2.

1.2 Stage 2: Tsunami Inundation Modelling

To model tsunami inundation, we used the set of nested elevation grids of increasing resolution approaching the area of interest from Burbidge et al. (2021), described further in Section 3.3 of this report. Then, for each of the scenarios identified in Stage 1, we used this set of nested grids to model the tsunami inundation all around Wellington Harbour. These models were run on the High Performance Computers (HPCs) hosted with New Zealand's eScience Infrastructure (NeSI). This is also described further in Section 3.

1.3 Stage 3: Probabilistic Hazard Maps

Finally, from this set of scenarios, we created probabilistic tsunami hazard maps showing the inundation extent and flow depths in the area of interest at each of the APoEs and sea-level values specified, following the method in Burbidge et al. (2021). Results are described in Section 4.

2.0 SCENARIO SELECTION

2.1 Deaggregating the National Tsunami Hazard Model

As stated earlier, the method used to select the scenarios is identical to the method described in Burbidge et al. (2021). This section is therefore identical to the corresponding section in that report. We repeat it here to ensure that this project's report includes details about the method used and can be a stand-alone document.

To calculate the scenarios for both the WCC and HCC projects, we have based the scenarios for inundation modelling on an updated NTHM.

This new model has a variety of improvements; the main one relevant for this project is improved modelling of the tsunami from local sources. To achieve this improvement in the treating of local sources, we modelled tsunami caused by 248 local faults from around New Zealand based on estimates of fault geometry and plausible magnitudes of the earthquakes that could occur on each fault (Stirling et al. 2012; Power 2013). We also updated data and methods used in calculating tsunami heights from local-, regional- and distant-source subduction zones. This is further detailed in Power et al. (in prep).

Figure 2.1a shows the updated hazard curves for Zone 91 in the new NTHM (Power et al., in prep). For comparison, the hazard curves from the 2013 NTHM (Power 2013) are also shown. The solid black line is the median hazard (as defined by the maximum offshore amplitude, a.k.a. tsunami height) as a function of the return period, while dashed lines show the 16% and 84% confidence intervals. The 16% and 84% confidence curves give an indication of the level of uncertainty in the hazard values for a given return period. Statistically, there is a 16% chance the hazard will be below the lower dotted line and an 84% chance it will be below the higher dotted line (and thus a 16% chance it will be above it). The level of uncertainty increases as we move to longer return periods. The return period here is the inverse of the APoE, and so we are more confident about more frequent (lower return period) hazard values than less frequent (higher return period) hazard values.

In the case shown here, the revised hazard estimated for Tsunami Hazard Zone 91 has gone down. This is mostly due to more accurate modelling of tsunami from South America and from local upper-plate faults in the Cook Strait region.

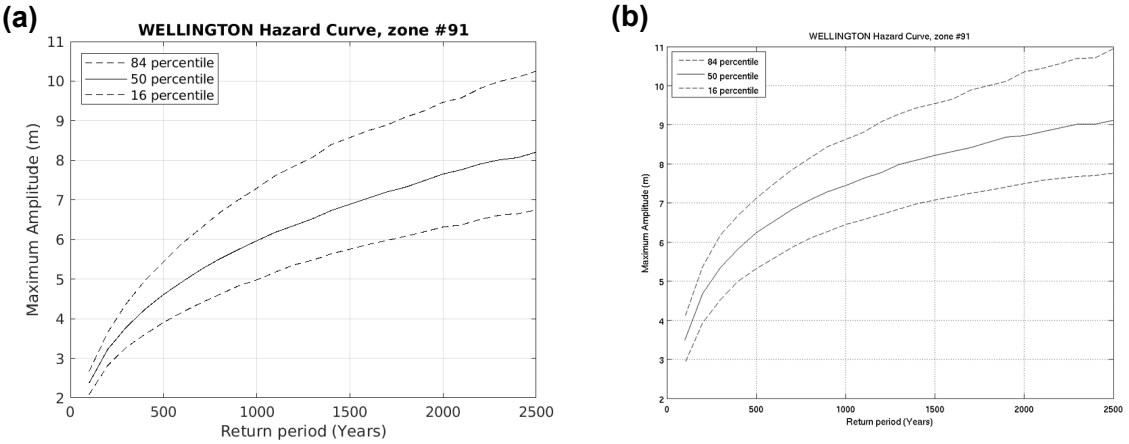

Figure 2.1 Tsunami hazard curves for Zone 91 in (left) the updated National Tsunami Hazard Model (NTHM; Power et al., in prep) and (right) 2013 NTHM (Power 2013). The offshore tsunami height (i.e. amplitude in the figure) above mean sea level is a function of the return period (inverse of the APoE).

The hazard at any particular APoE usually comes from a range of different earthquake sources. To determine this, we use a process known as 'deaggregation' to determine which sources contribute most of the hazard at a given APoE. Tables 2.1, 2.2 and 2.3 show the top six hazard source scenarios for each of the three APoEs for Zone 91 from this deaggregation. These sources encompass the majority of the hazard for that particular APoE in Zone 91. The locations of the earthquake sources are shown in Figure 2.2.

2.2 Determining the Earthquake Source Parameters

In order to determine the earthquake source parameters of each of the scenarios selected for tsunami inundation modelling, we first found a scenario in the database that produced a tsunami height in Tsunami Hazard Zone 91 closest to the tsunami height (target height) of a given APoE and that had a magnitude similar to the deaggregated scenario. We then scaled the slip amount based on the tsunami heights of the selected scenario (initial height) and the target height. The target height, initial slip amount and re-scaled slip and resulting moment magnitudes for each of three APoEs are shown in the following tables. To calculate the re-scaled slip amount, we multiplied the initial slip amount with the ratio between the target and initial height. The re-scaled slip amount can be used to calculate the re-scaled moment magnitude (Mw) by first re-calculating the scalar seismic moment (mo) while keeping the rigidity and fault area the same as the initial model values, using Equations 2.1 and 2.2.

$$mo = \mu SA \qquad \text{Equation 2.1}$$

$$Mw = \frac{2}{3}(log(mo) - 9.1) \qquad \text{Equation 2.2}$$

The assumed rigidity (μ) is 40 GPa for interplate and outer-rise earthquakes and 34.3 GPa for crustal fault earthquakes, while A is the fault area. These values were chosen to be consistent with values used in other studies, such as Gusman et al. (2019b) and Power et al. (in prep). The re-scaled slip and magnitudes for all of the deaggregated scenarios are presented in the following tables.

Table 2.1 Deaggregated source scenarios and the re-scaled slip and magnitude amount used in the inundation modelling for the 1:100-year annual probability of exceedance.

Source Name	Target Height (m)	Effective Moment Magnitude (from Deaggregation)	Initial Height (m)	Initial Slip Amount (m)	Re-Scaled Slip Amount (m)	Re-Scaled Moment Magnitude
Hikurangi	2.3704	8.086	2.34	2.77	2.81	8.0
Peru	2.3704	9.3435	2.30	19.59	20.22	9.31
Jordan, Kekerengu and Needles	2.3704	7.648	2.12	3.84	4.29	7.63
Northern Chile	2.3704	9.1985	1.90	19.96	24.94	9.16
Central Chile	2.3704	9.518	2.62	36.88	33.38	9.47
Kermadec	2.3704	9.07	2.48	21.5	20.53	9.09

Table 2.2 Deaggregated source scenarios and the re-scaled slip and magnitude amount used in the inundation modelling for the 1:500-year annual probability of exceedance.

Source Name	Target Height (m)	Effective Moment Magnitude (from Deaggregation)	Initial Height (m)	Initial Slip Amount (m)	Re-Scaled Slip Amount (m)	Re-Scaled Moment Magnitude
Hikurangi	4.61	8.567	5.83	3.83	7.01	8.55
Jordan, Kekerengu and Needles	4.61	7.936	5.43	2.95	8.49	7.93
Wairarapa and Wharekauhau	4.61	8.254	18.96 and 3.23	5.34	16.38 and 2.79	8.26
Hope and Te Rapa	4.61	7.76	4.22	3.04	6.4	7.72
Wairarapa	4.61	8.29	18.96	4.93	17.75	8.28
South Wairarapa Outer Rise	4.61	8.327	10.47	3.52	13.72	8.28

Table 2.3 Deaggregated source scenarios and the rescaled slip and magnitude amount used in the inundation modelling for the 1:1000-year annual probability of exceedance.

Source Name	Target Height (m)	Effective Moment Magnitude (from Deaggregation)	Initial Height (m)	Initial Slip Amount (m)	Re-Scaled Slip Amount (m)	Re-Scaled Moment Magnitude
Hikurangi	5.96	8.69	6.41	3.83	9.37	8.68
Jordan, Kekerengu and Needles	5.96	8.05	5.43	2.95	10.99	8.00
Wairarapa and Wharekauhau	5.96	8.365	18.96 and 3.23	5.34	21.18 and 3.61	8.33
Wairarapa	5.96	8.40	18.96	4.93	22.95	8.36
Hope and Te Rapa	5.96	7.871	4.22	3.04	8.28	7.80
South Wairarapa Outer Rise	5.96	8.44	10.47	3.52	17.74	8.35

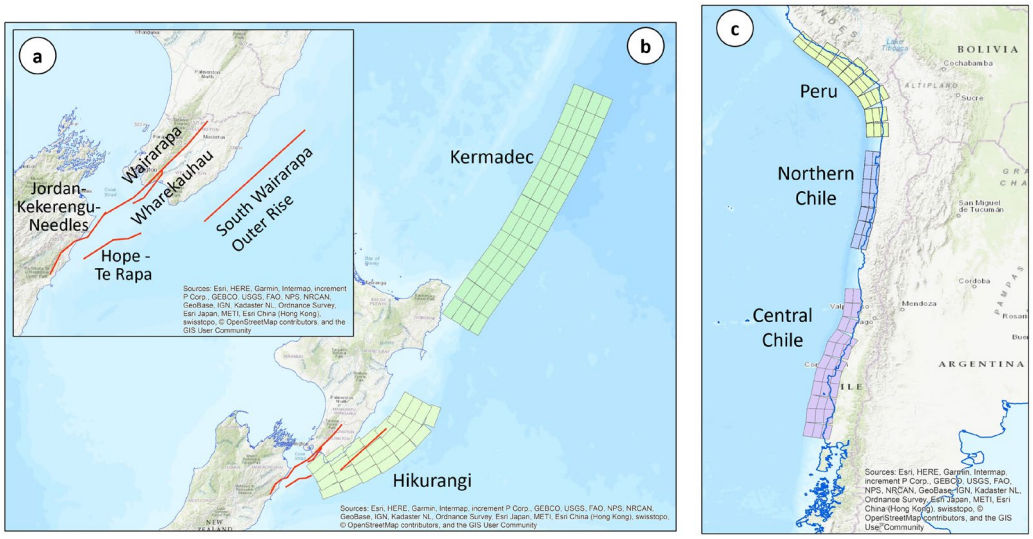

Figure 2.2 Earthquake source model locations. (a) Local upper-plate faults traces (red lines) used for the hazard model. (b) Sub-fault patches used for the Kermadec and Hikurangi earthquake source models. (c) Sub-fault patches used for the Peru, Northern Chile and Central Chile source models.

3.0 TSUNAMI INUNDATION MODELLING

3.1 Simulation Software: COMCOT

The numerical simulation model, COMCOT (**CO**rnell **M**ulti-grid **CO**upled **T**sunami), was adopted to simulate tsunami generation and propagation from their sources to Wellington Harbour, calculate tsunami evolution inside the harbour and model detailed tsunami inundations in the coastal areas. The model was originally developed at Cornell University, USA, in the 1990s (Liu et al. 1998; Wang 2008) and, since 2009, it has been under development at GNS Science, New Zealand (Wang and Power 2011). Multiple source mechanisms have been integrated in this simulation tool, such as earthquakes with time-dependent rupture, variable slip distributions or landslides.

This model has been widely benchmarked and used by researchers worldwide to study various aspects of tsunami, including tsunami-generation mechanisms, transoceanic propagation, run-up and coastal inundation. In recent years, it has been further developed and is increasingly used to investigate storm surges; wave-structure interactions; effects of rivers, tides and sea-level rise on tsunami hazards; landslides in reservoirs/lakes; and downstream flooding (Wang and Liu 2006; Wijetunge et al. 2008; Beavan et al. 2010; Wang 2008, Wang and Power 2011; Mueller et al. 2015a; Wang et al. 2017a, 2017b; Mountjoy et al. 2019; Liu et al. 2018; Li et al. 2018; Mueller et al. 2019; Power et al. 2019; Wang et al. 2020a, 2020b). The latest version of this model was used in this study.

COMCOT uses a modified staggered finite difference scheme to solve linear and non-linear shallow water equations that typically govern tsunami, floods and river flows with shock[1] capturing up-wind schemes, together with ad-hoc wave breaking algorithms (Kennedy et al. 2000; Lynett 2002; Wang and Power 2011) for improved stability and to account for the energy dissipation effects during run-up and inundation. Both spherical and Cartesian coordinate systems are supported, providing flexibility to tsunami hazard investigations over large transoceanic coverages and small local areas. A two-way nested grid configuration is implemented in the model to balance computational efficiency and numerical accuracy (Wang 2008; Wang and Power 2011). The model uses a relatively large grid spacing to efficiently simulate the propagation of tsunami in the deep ocean and switches to refined grid spacings in nearshore and coastal regions to account for the shortening of tsunami wave length due to the shallowness of water depth and to achieve sufficient numerical accuracy in the areas of interest (Fraser 2014; Fraser et al. 2014).

3.2 Reference Level and Terminologies

COMCOT uses a universal reference level (zero-elevation level), locally in coincidence with Mean Sea Level (MSL), to interpret input data for elevation information in the Digital Elevation Model (DEM) and create output data such as tsunami elevations. This reference level is fixed in a virtual space, does not change throughout a numerical simulation and, particularly, is not affected by any potential co-seismic displacements (e.g. uplift or subsidence) in a local earthquake event. During a simulation and in output data, tsunami elevation is defined as the

1 This is a modelling method to deal with shock waves in inviscid fluids (common assumption for water for gravity-dominated wave dynamics modelling). Shock waves will lead to a sharp of fluid motions, causing discontinuities of flow variables, a major source of instability. COMCOT uses a conservative form of governing equations so that shock waves become a natural part of the solution. Accuracy and stability are further enhanced by specially designed up-wind finite difference schemes in which no information in front of a shock ('unknown zone') will be used to evaluate derivatives, based on velocity directions.

tsunami water surface level above the universal reference level (e.g. MSL); tsunami flow depth refers to the vertical water layer thickness between the water surface and the topographical surface (ground or seafloor surface) as defined in the DEM (Figure 3.1). Elevation data is positive if above the universal reference level (in this case, tsunami elevation is often called tsunami height) and negative if below it. Note that flow depth values are independent of reference levels.

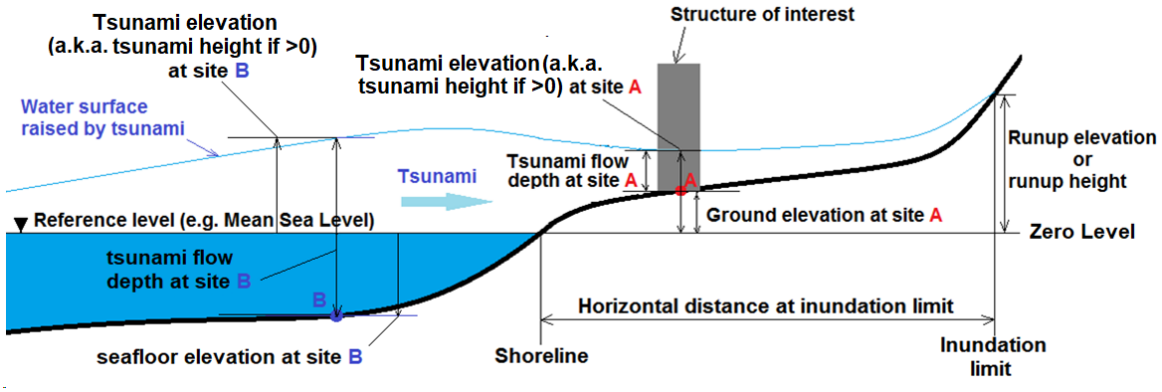

Figure 3.1 Illustration of some definitions used in tsunami modelling, for example, water surface level / tsunami elevation (i.e. tsunami height), tsunami flow depth / inundation depth and ground elevation at site location A on land and B in water.

3.3 Digital Elevation Model Data

Three sets of DEM data have been used in this study to meet spatial accuracy and coverage requirements for the simulation of tsunami originating from their sources, travelling through open sea and interacting with the coasts of Wellington Harbour and its surrounding areas. These DEM datasets are:

- Global DEM data
- New Zealand DEM data, and
- Wellington Harbour DEM data.

These DEM datasets provide elevation information at numerical modelling grids used for the tsunami simulations (see Section 3.4).

3.3.1 Global Digital Elevation Model

Global DEM data was developed at a spatial resolution of 2 arc-minutes (~3600 m on the equator and ~2700 m in Wellington) using ETOPO2v2 (https://www.ngdc.noaa.gov/mgg/global/etopo2.html) as a base model, together with other data. ETOPO2v2 is a 2 arc-minute global relief model of Earth's surface that integrates land topography and ocean bathymetry and is available from the National Centre for Environmental Information of NOAA (National Oceanic and Atmospheric Administration). In addition to this dataset, the New Zealand DEM data was used to update the New Zealand region in the original ETOPO2v2 data for improved data accuracy.

3.3.2 New Zealand Digital Elevation Model

The New Zealand DEM data was derived from LINZ Charts, the Seabed Mapping CMAP, GEBCO 08 (https://www.gebco.net/news_and_media/updated_gebco_08_release.html) and LINZ 8 m elevation datasets. This DEM dataset covers the main islands of New Zealand and their offshore regions at a grid spacing of 10 arc-seconds (~200–250 m in New Zealand).

3.3.3 Wellington Harbour Digital Elevation Model

This 10 m high-resolution DEM data covers the Wellington Harbour and its surrounding suburbs. This data was initially created for hydrodynamic inundation modelling and delineation of tsunami evacuation zones for Wellington Harbour (Mueller et al. 2015b) and was derived from a combination of LiDAR topographic data provided by Wellington Regional Council and multi-beam bathymetric survey data provided, with permission, from NIWA (Pallentin et al. 2009) covering the interior of the harbour. Outside the harbour, the bathymetric data was derived from LINZ nautical charts. It was further developed in Burbidge et al. (2021) for the WCC tsunami hazard map project using new LiDAR provided by WCC. For further details, see Burbidge et al. (2021).

3.4 Modelling Grid Set-Up

The COMCOT tsunami modelling software uses a series of nested numerical modelling grids at cascading spatial resolutions to account for spatial resolution requirements by a tsunami travelling in different regions, e.g. from deep ocean basin to shallow coastal areas (Wang and Power 2011). In this study, five levels of numerical grid with different spacing refinement were used to simulate tsunami generation, transoceanic propagation, coastal run-up and inundation. This nested grid set-up is able to telescope spatial resolutions from 2 arc-minutes (~3600 m on the Equator), covering the entire Pacific, to 0.5 arc-seconds (about 11 metres) covering the Wellington Harbour and its surrounding areas.

The first grid level (grid 01) covers the whole Pacific Ocean and is used to simulate tsunami generation and propagation from sources around the Pacific to New Zealand. It has a spatial resolution of 2 arc-minutes (~3600 m on the Equator and ~2700 m in Wellington, see Figure 3.2). The elevation data of grid 01 was interpolated from the Global DEM data, as described in Section 3.3.1.

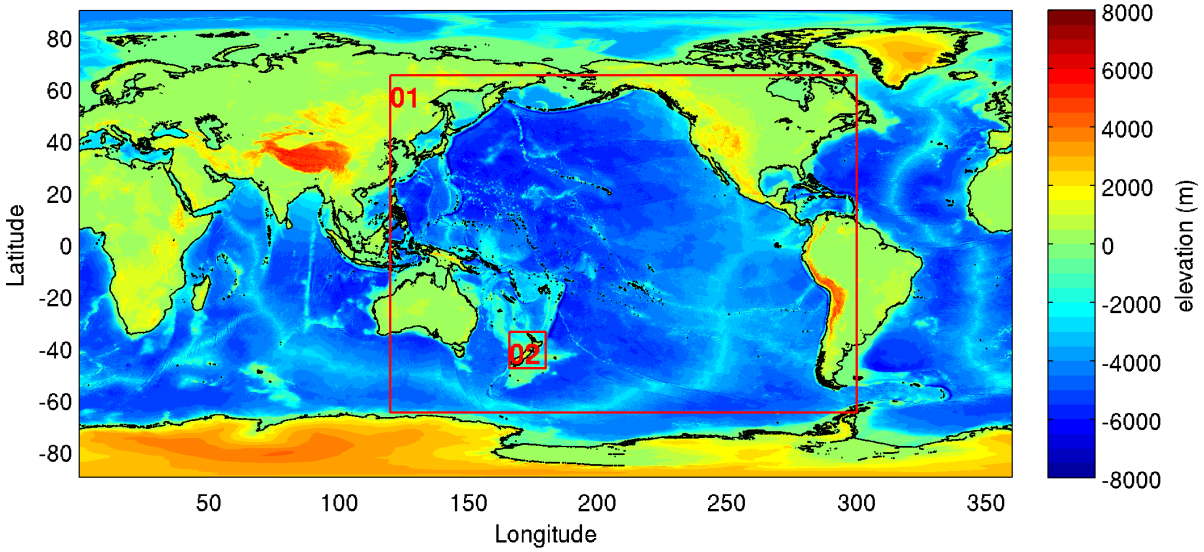

Figure 3.2 Global digital elevation model grids at a spatial resolution of 2 arc-minutes and the coverage used for the inundation modelling. Red boxes outline the coverages of grids 01 and 02. Elevation (relative to MSL) is colour-coded in metres.

The second grid level (grid 02) covers New Zealand's main islands and their offshore regions at 30 arc-seconds (~640–740 m in New Zealand and ~675 m in Wellington). The area covered by this grid is shown in Figure 3.2. The third grid level (grid 03) covers the Cook Strait region, including southern North Island and northern upper South Island at a spatial resolution of

6.0 arc-seconds (~135 m in Wellington), as shown in Figure 3.3. The fourth grid level (grid 04) covers the south of the North Island and the sea in front of it at a spatial resolution of 1.5 arc-seconds, about 34 m in Wellington. The area covered by this grid is shown in Figure 3.3. The elevation data of grids 02 to 04 were all interpolated from the 10 arc-second New Zealand DEM data, as described in Section 3.3.2.

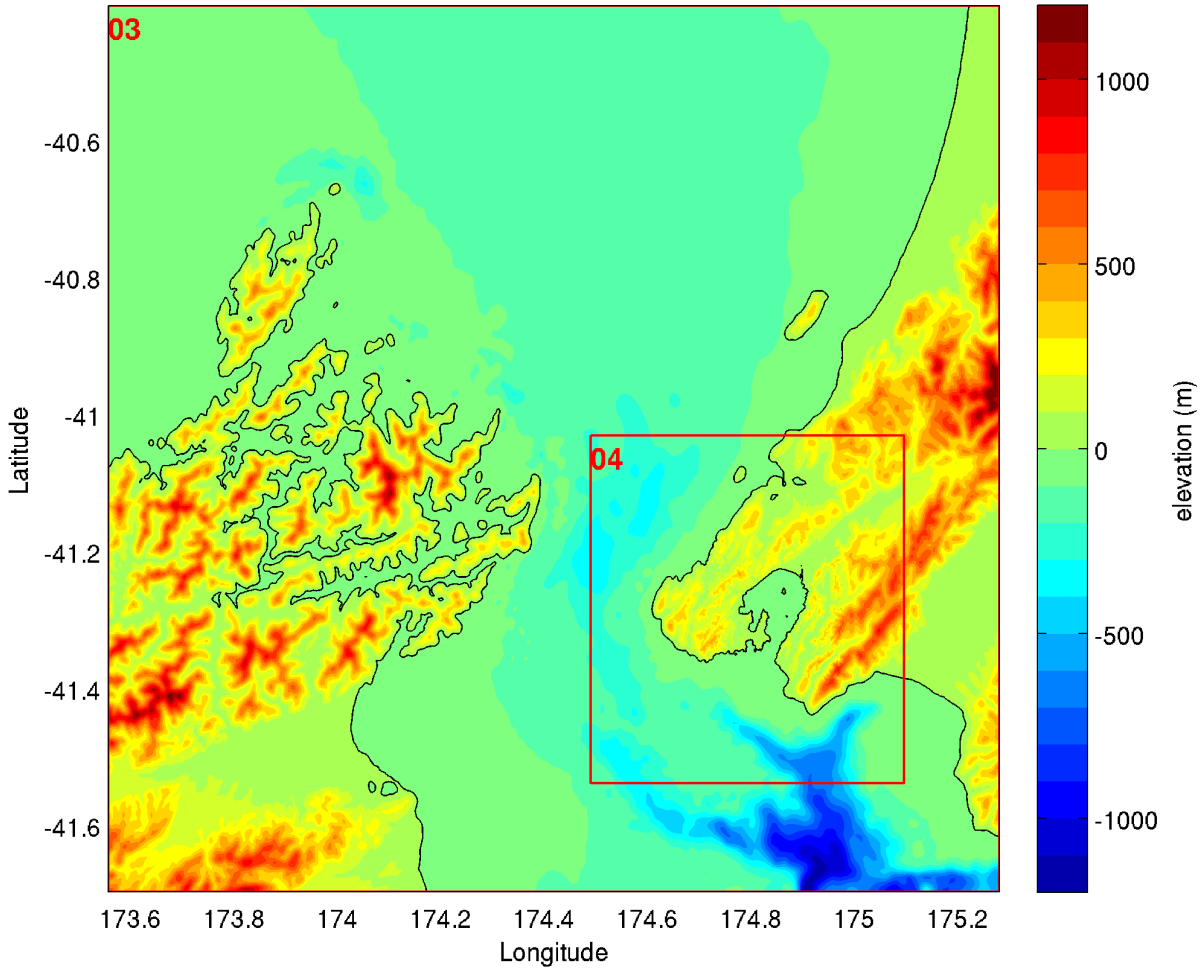

Figure 3.3 Coverage of grids 03 and 04. The Digital Elevation Model shown is from grid 03 and is at a spatial resolution of six arc-seconds. The red box outlines the area covered by grid 04. Elevation (relative to MSL) is colour-coded in metres.

The fifth, and final, grid level (grid 05) covers the entire Wellington Harbour and its surrounding suburbs at a grid spacing of about 11 m for the high-resolution inundation modelling (Figure 3.4). Its elevation data was interpolated from the Wellington Harbour DEM.

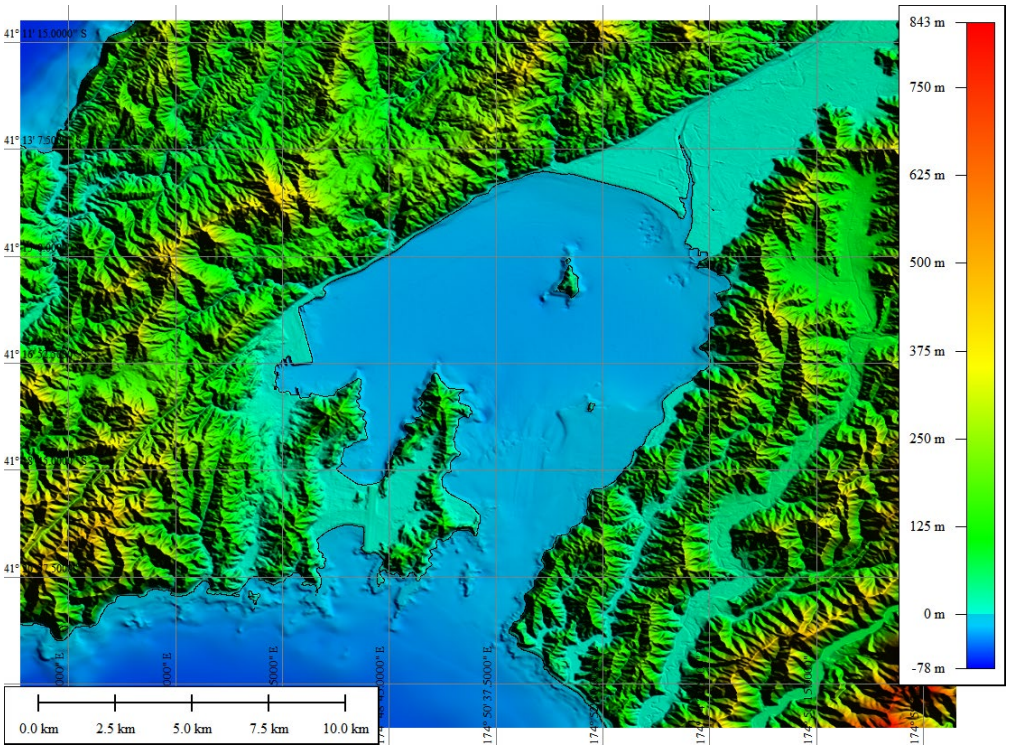

Figure 3.4 Coverage of modelling grid 05, which has the highest level of detail for the modelling of tsunami interactions in the Wellington Harbour region and coastal inundation of Wellington. Elevation (relative to MSL) is colour-coded in metres. Wellington Harbour bathymetry (1 m digital grid) includes high-resolution bathymetric data provided by NIWA (Pallentin et al. 2009).

Table 3.1 summarises the nested grid set-up and modelling settings used for this study.

Table 3.1 Nested grid set-up for tsunami simulations. The grid sizes are indicative, only accurate along parallels of latitude; refer to Section 3.6 for further detail about grid sizes.

Grid	Grid Coverage	Grid Size (Arc-Second)	Time Step (Second)	Tsunami Model	Boundary Condition
01	120.0~300.0E, -65.0~65.0N	120.00 (~2700 m)	3.2512	Linear	Absorbing
02	166.0~180.0, -48.0~-34.0	30.00 (~675 m)	1.6256	Linear	2-way nested
03	173.559~175.283, -41.696~-40.403	6.00 (~135 m)	0.5419	Linear	2-way nested
04	174.491~175.100, -41.539~-41.031	1.50 (~34 m)	0.2709	Linear	2-way nested
05	174.704~174.979, -41.388~-41.181	0.50 (~11 m)	0.1355	Non-linear	2-way nested
05	174.704~174.979, -41.388~-41.181	0.50 (~11 m)	0.1355	Non-linear	2-way nested

3.5 Roughness Model

In tsunami inundation modelling, a commonly adopted approach is that land-cover features, such as buildings, are deliberately removed from DEM data and replaced with corresponding equivalent roughness values for different types of land covers (Wang et al. 2017a and references therein). It is also preferable that a range of roughness values are used for different land-cover types in an inundation simulation in order to account for the spatial variation of their resistance effects on tsunami flow dynamics.

In this study, we used a set of roughness values (i.e. Manning's roughness coefficient, n; Manning 1891) for a relatively simplified set of land-cover groups proposed in Wang et al. (2017a). The land-coverage groups and their roughness values are given in Table 3.2. These values were derived by comparing roughness values found in the literature, grouping and averaging roughness values for similar land-cover types (Arcement et al. 1984; Fujima 2001; Imamura et al. 2006; Wang and Liu 2007; Wang et al. 2009; Gayer et al. 2010; Kaiser et al. 2011; Fraser et al. 2014; Bricker et al. 2015) but leaning slightly toward the lower end of the value ranges.

Table 3.2 Roughness values for different land-cover groups for the tsunami modelling.

Land-Cover Group	**Manning's n (Roughness Coefficient)**
Built-up area (e.g. urban / residential / industrial / Central Business District)	0.060
Tall vegetation (e.g. forest)	0.040
Scrub (e.g. low trees / bushes)	0.040
Low vegetation (e.g. grass)	0.030
Urban open area (e.g. paved/smoothed)	0.025
Bare land (e.g. farmland)	0.025
Water area (e.g. riverbed/seabed)	0.011

Figure 3.5 shows the spatial distribution of roughness values (Manning's n) for different land-cover groups in the Wellington Harbour and its surrounding areas.

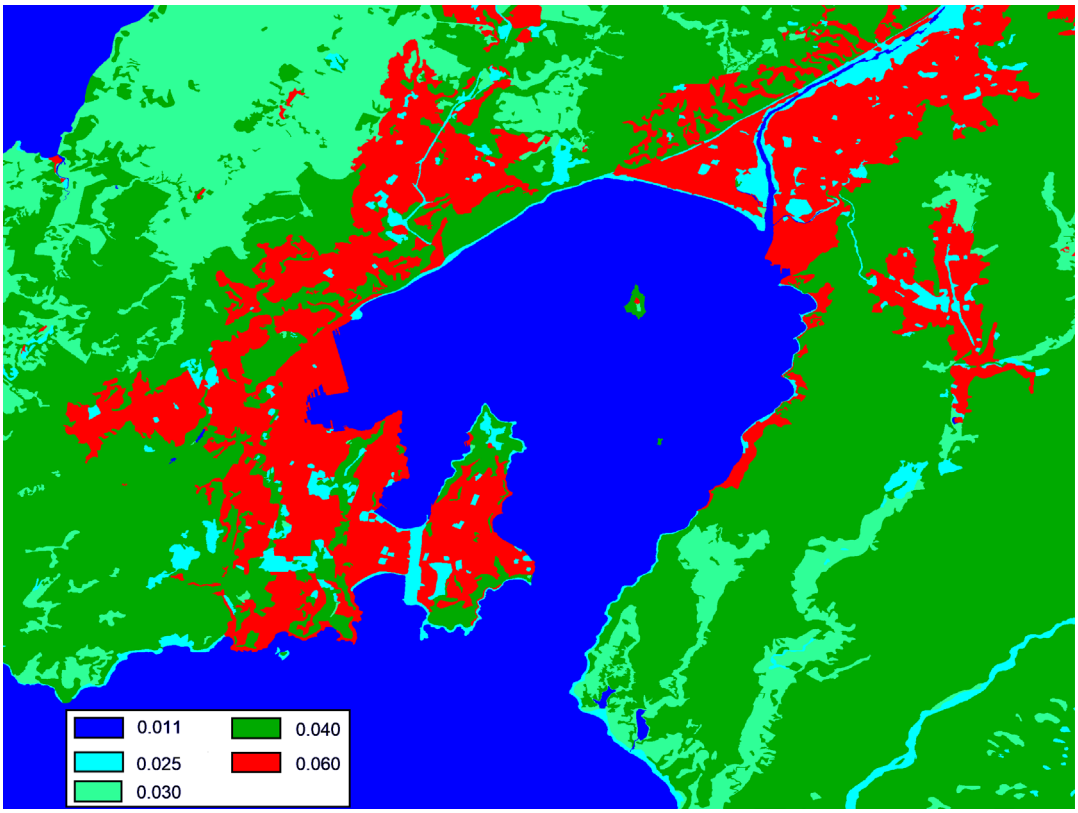

Figure 3.5 Spatial distribution of equivalent surface roughness values, i.e. Manning's n, in Wellington for tsunami inundation modelling.

3.6 Effects of Earth Curvature, Rotation and High Latitude

This study adopts tsunami governing equations in a Spherical Coordinate System to simulate tsunami from selected sources to the Wellington Harbour region. This is necessary for tsunami simulations over a very large area that needs to consider the curvature of the Earth's surface. The effect of the Earth's rotation was also evaluated through the inclusion of the Coriolis force in both linear and non-linear tsunami models in COMCOT (Wang and Power 2011).

In high-latitude regions, the commonly-used approach of using 'square' grids in spherical coordinates, i.e. equal cell edges in arc-degrees, leads to grid cells that are highly elongated when measured in metres. For example, for this type of grid in Wellington, the south–north edge of a grid cell will be over 30% longer than its west–east edge. This will not only affect the stability of tsunami simulations but also lead to inconsistent accuracies of modelling results in different directions.

To overcome these issues, the size of a numerical grid cell in COMCOT varies along its meridian (i.e. lines of longitude) and is self-adjusted according to its latitude so that its edge length along the parallel (i.e. circles of latitude) and meridian are equal in metres. This ensures that 'square' grids (in metre terms) are created for numerical calculations and thus maintains the same accuracies in different directions. As a result, the grid sizes given in Table 3.1 are nominal and are only true along the parallels.

3.7 Other Simulation Settings

In the tsunami simulations, co-seismic ground surface and seafloor displacement in an earthquake event is calculated using the widely used elastic finite fault theory of Okada (1985) and is introduced in the model as the initial condition of tsunami generation.

In local earthquake events, the co-seismic uplift or subsidence may also change the ground and seafloor elevation as defined in the input DEM (i.e. current-day DEM or pre-event DEM). When this happens, the COMCOT model firstly adjusts the input DEM with the computed co-seismic uplift/subsidence and then simulates the subsequent tsunami to calculate hazard parameters, e.g. tsunami elevation, flow depth, flow velocity and flow acceleration, over the adjusted DEM (i.e. post-event DEM).

In the numerical simulations, tsunami propagation was simulated for 25 hours for distant scenarios (e.g. South America), 15 hours for regional scenarios (e.g. Kermadec), and 10 for local earthquake scenarios (e.g. Hikurangi, New Zealand crustal faults) from their generation in the sources to ensure that the maximum tsunami hazard parameters were obtained in the Wellington Harbour region. Detailed examinations of selected scenarios revealed that the maximum tsunami inundation extents had clearly been reached in less than 10 hours after first arrivals, reassuring that these run times were long enough. All of the simulations assume that tsunami occurs at MHWS or at MHWS plus 1.0 m of sea-level rise. MHWS was modelled as a static level of 0.69 m above local MSL, not changing over time with the tide fluctuations.

3.8 Final Models

For each of the scenarios indicated in Table 2.1, we ran the models through all of the grids to inundation on the last level (grid 05). An example of one of them is shown in Figure 3.6. It shows the inundation produced by a M_W 8.7 earthquake on the Hikurangi subduction zone. This was one of the scenarios that contributed to the hazard at an APoE of 1:1000 years. This particular scenario causes one of the largest amounts of inundation in the area of interest.

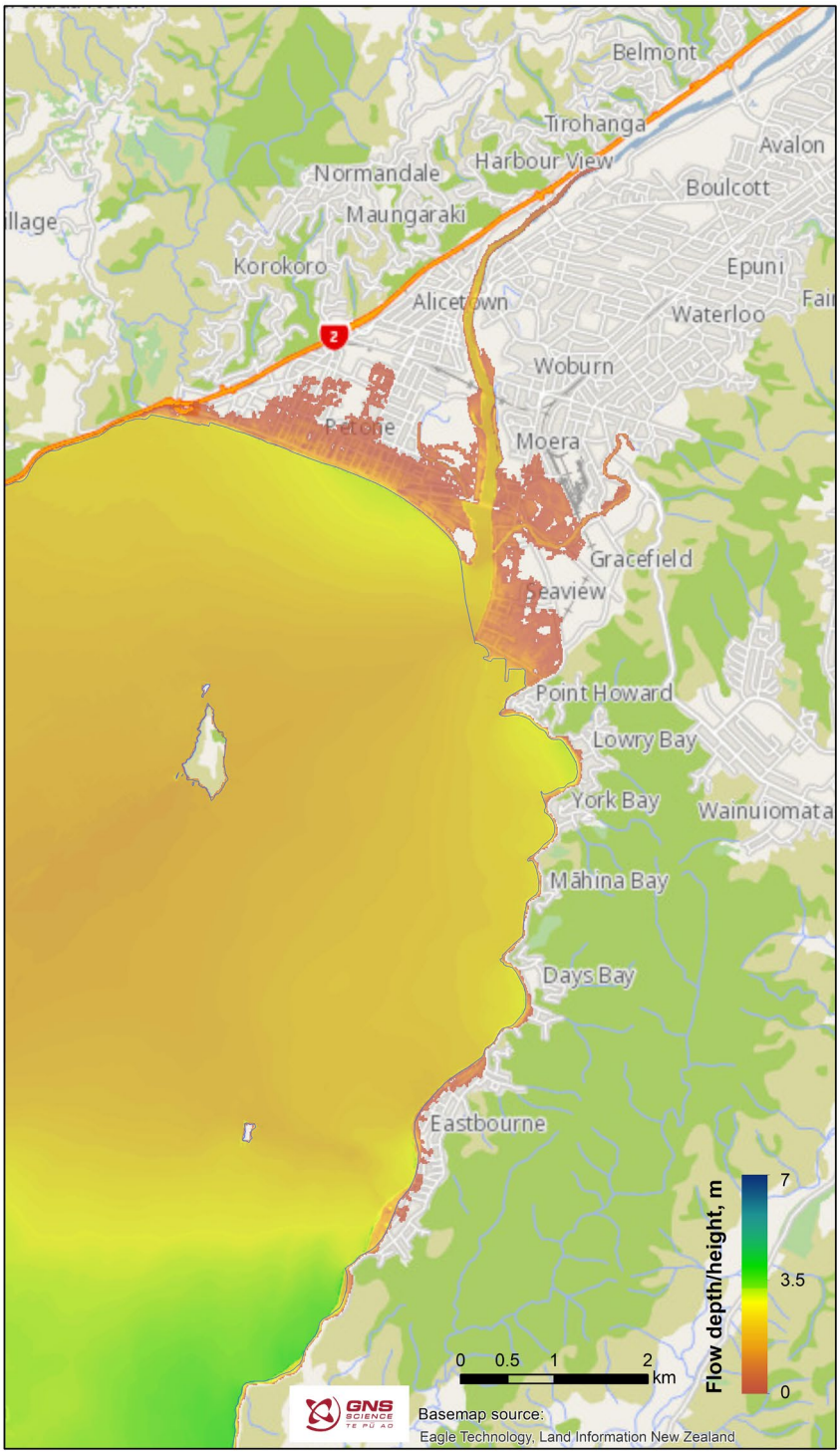

Figure 3.6 Example of the inundation produced from a M_W 8.7 event on the Hikurangi subduction zone. Onshore values refer to flow depths, while offshore values refer to maximum tsunami heights.

4.0 PROBABILISTIC TSUNAMI INUNDATION HAZARD MAPS

The contribution of each of the inundation scenarios were then normalised according to their contribution to the hazard (shown in Table 4.1 as 'Normalised contribution') and used to find the weighted median of flow depths across the area of interest. The 'Percentage of Deaggregation' describes how large a proportion that source represents in the total deaggregation. The 'Percentage of Top Sources' describes these proportions if the sources outside the top sources (in this case, the top six) are excluded – these six percentages then add up to 100%.

The resulting maps of median flow depths/heights are shown in Figures 4.1–4.6. As expected, regions with the largest inundation for a given APoE include the Petone, Moera, Seaview, Point Howard, Lowry Bay, York Bay, Mahina Bay, Days Bay and Eastbourne areas. Also as expected, the area inundated at the given APoE is larger when sea-level rise of 1.0 m is added to the current MHWS initial sea level. Broadly speaking, increasing the MHWS by 1.0 m increases the probability of a given extent of inundation. For example, the 1:500-year inundation hazard map without 1.0 m of sea-level rise has a similar inundation extent in most areas, and even a smaller extent in Seaview and Moera, to that in the 1:100-year APoE hazard map with the extra metre of sea-level rise included. In Seaview and Moera, the tsunami inundation extent increased more from the increase of sea level (e.g. from 1:100-year APoE with present sea level to the same APoE with 1.0 m sea-level rise) than from the increase in return period (e.g. from a 1:100-year APoE to a 1:500-year APoE).

The inundation area for the 1:100-year APoE is limited to the beaches and the Hutt River mouth. The 1:100-year APoE with a 1.0 m sea-level rise scenario inundated some low-lying areas and the riverbank in Petone, Moera, Seaview and Grassfield. The narrow low-laying areas next to the beaches between Point Howard and Eastbourne are inundated in the 1:100-year APoE with 1.0 m of sea-level rise, the 1:500-year APoE and the larger scenarios. The inundation area for the 1:500-year APoE in most coastal areas is slightly smaller than that from the 1:100-year APoE with 1.0 m of sea-level rise; moreover, the inundation in Seaview, Moera and Gracefield in the 1:500-year APoE is less severe. A significant part of Petone, Seaview and Moera is inundated in the 1:500-year APoE with 1.0 m of sea-level rise, and a large part of the riverbanks are inundated with flow depths up to almost 3 m on the river. The inundation area for the 1:1000-year APoE is slightly smaller than that for the 1:500-year APoE, with 1.0 m of sea-level rise. Most of Petone, Seaview, Moera and Eastbourne are inundated in the 1:1000-year APoE with 1.0 m of sea-level rise. In this most severe scenario of this study, part of the built area of Alicetown is also inundated.

The data used in the maps are provided to HCC in an ESRI Geodatabase as rasters of median flow depth/height and feature classes of tsunami inundation extent. All of the datasets are in WGS 1984 geographic coordinate system.

Table 4.1 Scenario normalised contribution.

Annual Probability of Exceedance	Source Name	Effective Magnitude	Percentage of Deaggregation	Percentage of Top Sources ('Normalised')
1:100	Hikurangi	8.086	39.33%	55.65%
1:100	Peru	9.3435	9.00%	12.73%
1:100	Jordan-Kekerengu-Needles	7.648	7.37%	10.42%
1:100	Northern Chile	9.1985	5.20%	7.36%
1:100	Central Chile	9.518	5.02%	7.10%
1:100	Kermadec	9.07	4.77%	6.74%
1:500	Hikurangi	8.567	36.03%	49.98%*
1:500	Jordan-Kekerengu-Needles	7.936	16.90%	23.44%
1:500	Wairarapa and Wharekauhau	8.254	5.50%	7.63%
1:500	Hope	8.254	5.20%	7.21%
1:500	Wairarapa	7.76	4.97%	6.89%
1:500	South Wairarapa Outer Rise	8.29	3.50%	4.85%
1:1000	Hikurangi	8.69	33.82%	43.41%
1:1000	Jordan-Kekerengu-Needles	8.05	18.55%	23.81%
1:1000	Wairarapa and Wharekauhau	8.365	8.17%	10.48%
1:1000	Wairarapa	8.365	7.25%	9.31%
1:1000	Hope	8.40	5.22%	6.70%
1:1000	South Wairarapa Outer Rise	7.871	4.90%	6.29%

* The 1:500 hazard map based on a weighted median would be altered if this was >50%, and such a small variation is within the random error of our method (see Section 5).

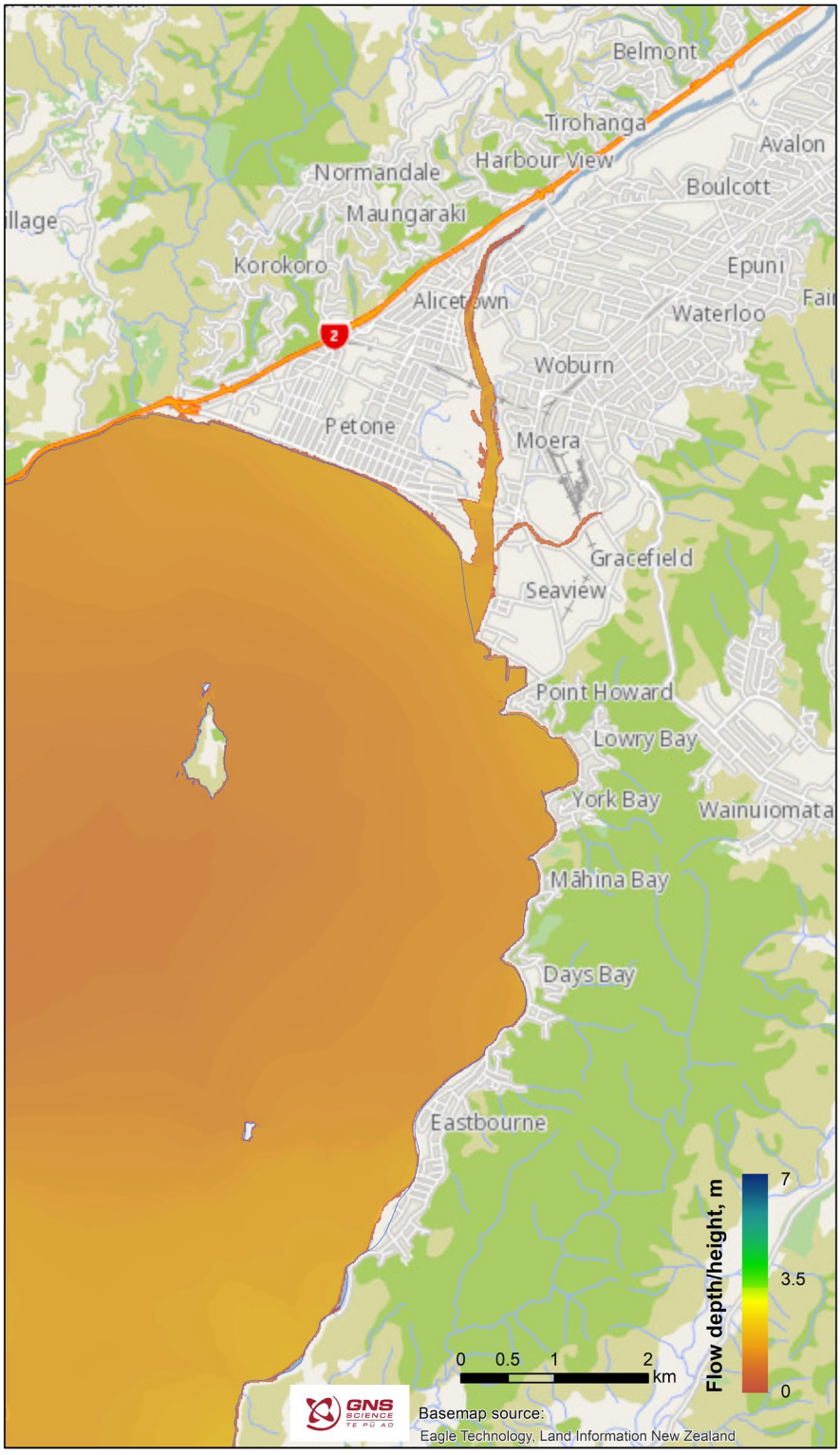

Figure 4.1 Probabilistic tsunami inundation map for Lower Hutt showing the median flow depths onshore and offshore tsunami heights with a 1-in-100-years chance of being exceeded per annum at current MHWS. Onshore values refer to flow depths, while offshore values refer to maximum tsunami heights.

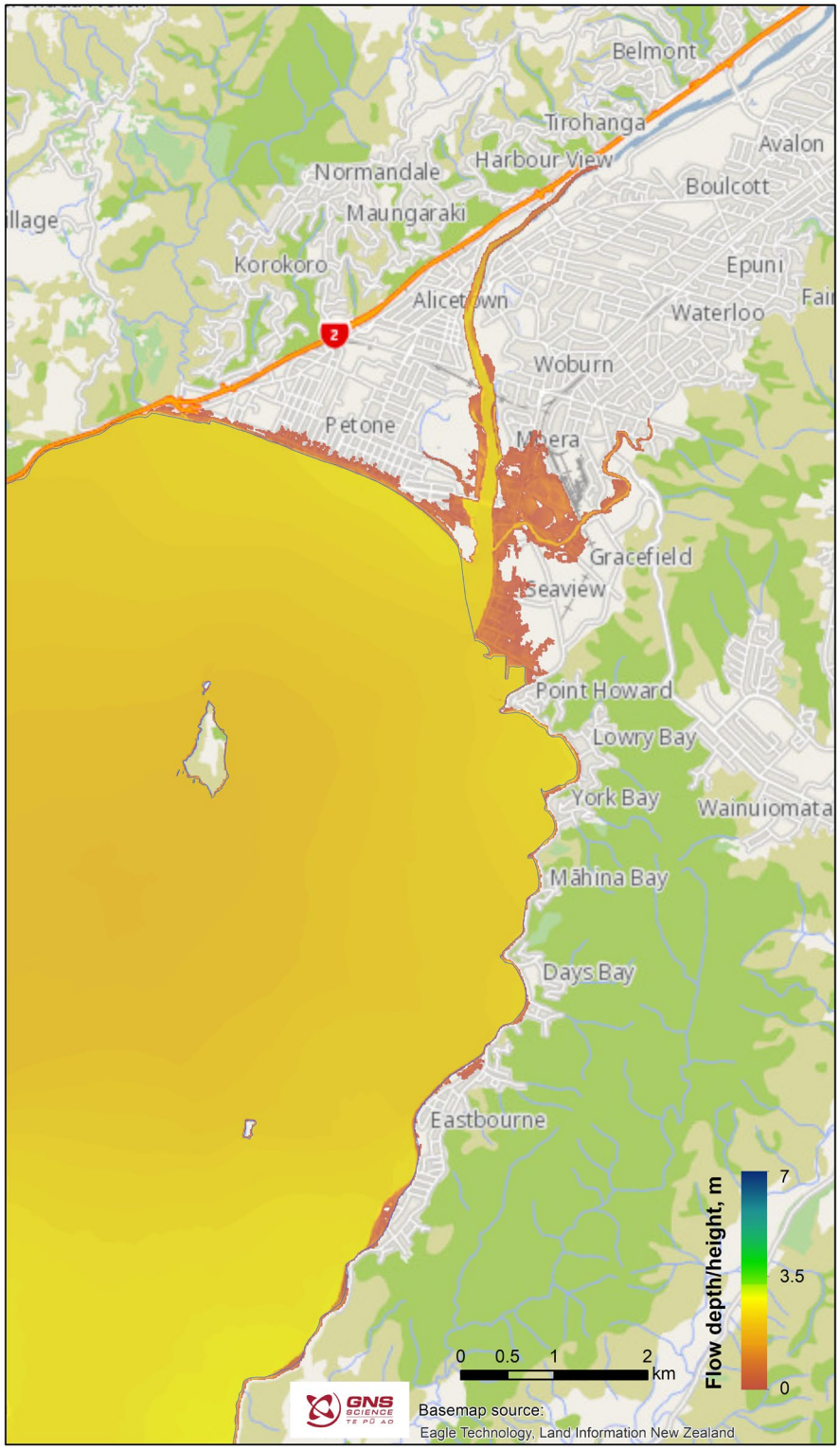

Figure 4.2 Probabilistic tsunami inundation map for Lower Hutt showing the median flow depths onshore and offshore tsunami heights with a 1-in-100-years chance of being exceeded per annum at current MHWS **plus 1.0 m of sea-level rise**. Onshore values refer to flow depths, while offshore values refer to maximum tsunami heights.

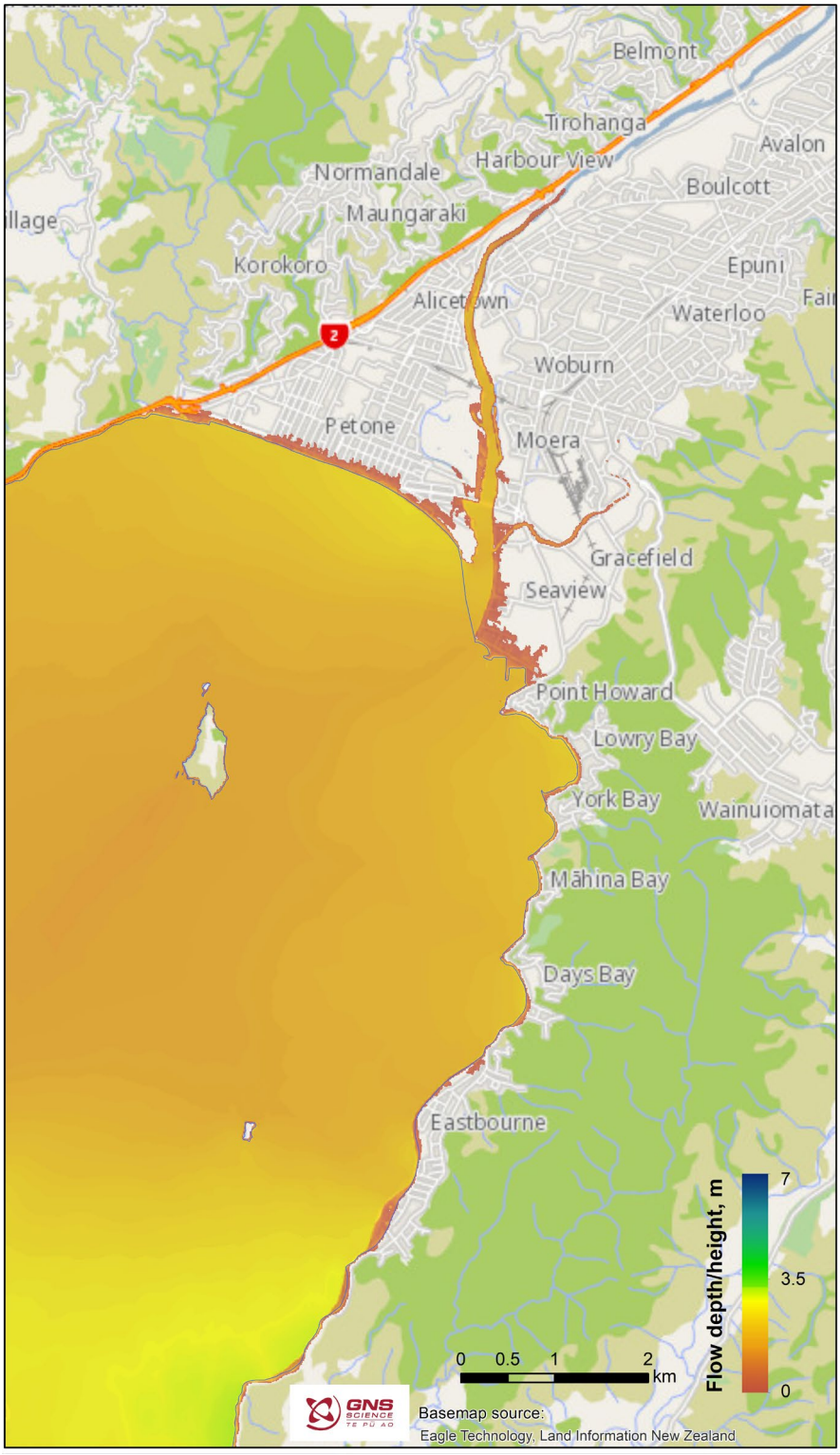

Figure 4.3 Probabilistic tsunami inundation map for Lower Hutt showing the median flow depths onshore and offshore tsunami heights with a 1-in-500-years chance of being exceeded per annum at current MHWS. Onshore values refer to flow depths, while offshore values refer to maximum tsunami heights.

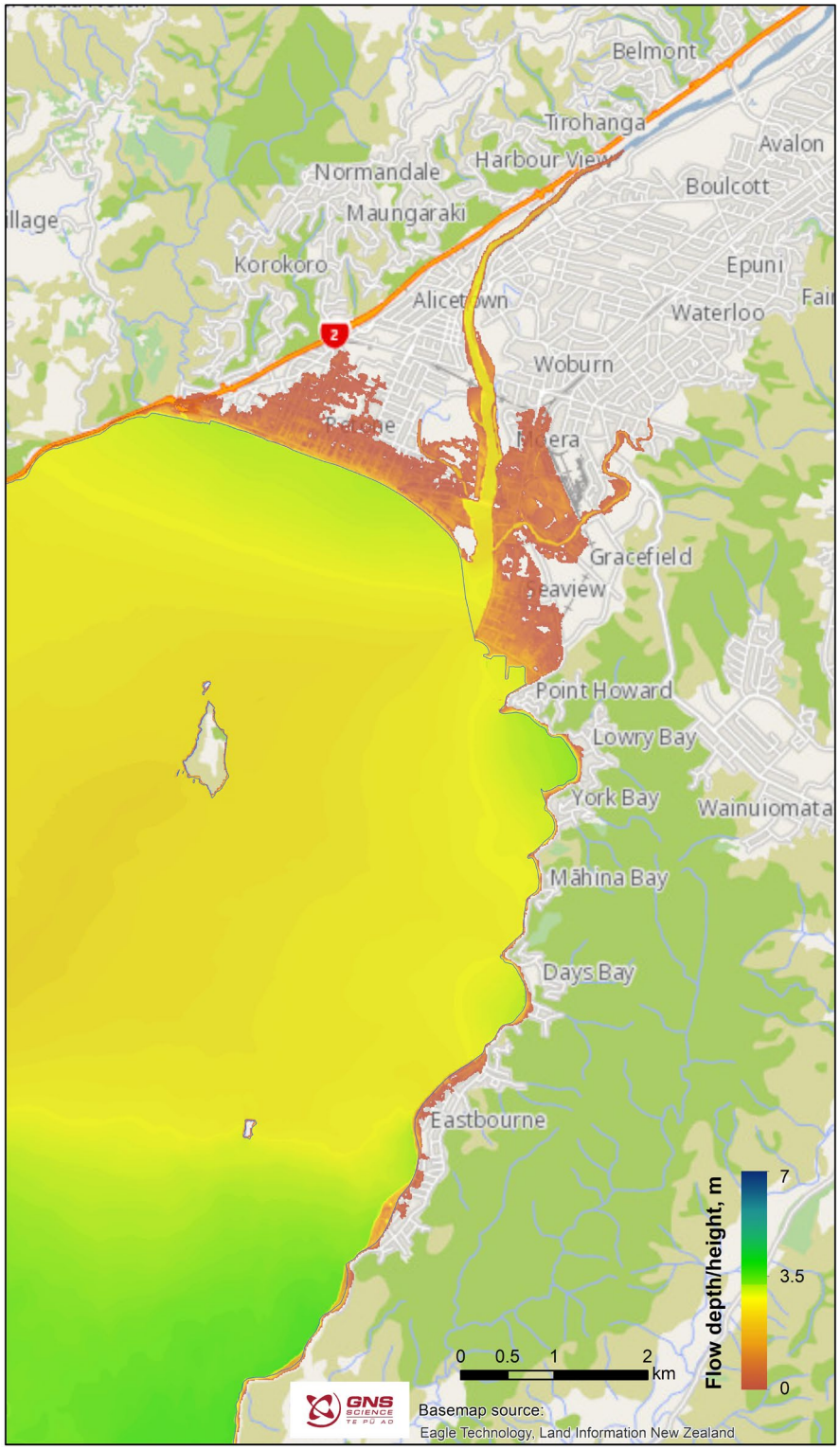

Figure 4.4 Probabilistic tsunami inundation map for Lower Hutt showing the median flow depths onshore and offshore tsunami heights with a 1-in-500-years chance of being exceeded per annum at current MHWS **plus 1.0 m of sea-level rise**. Onshore values refer to flow depths, while offshore values refer to maximum tsunami heights.

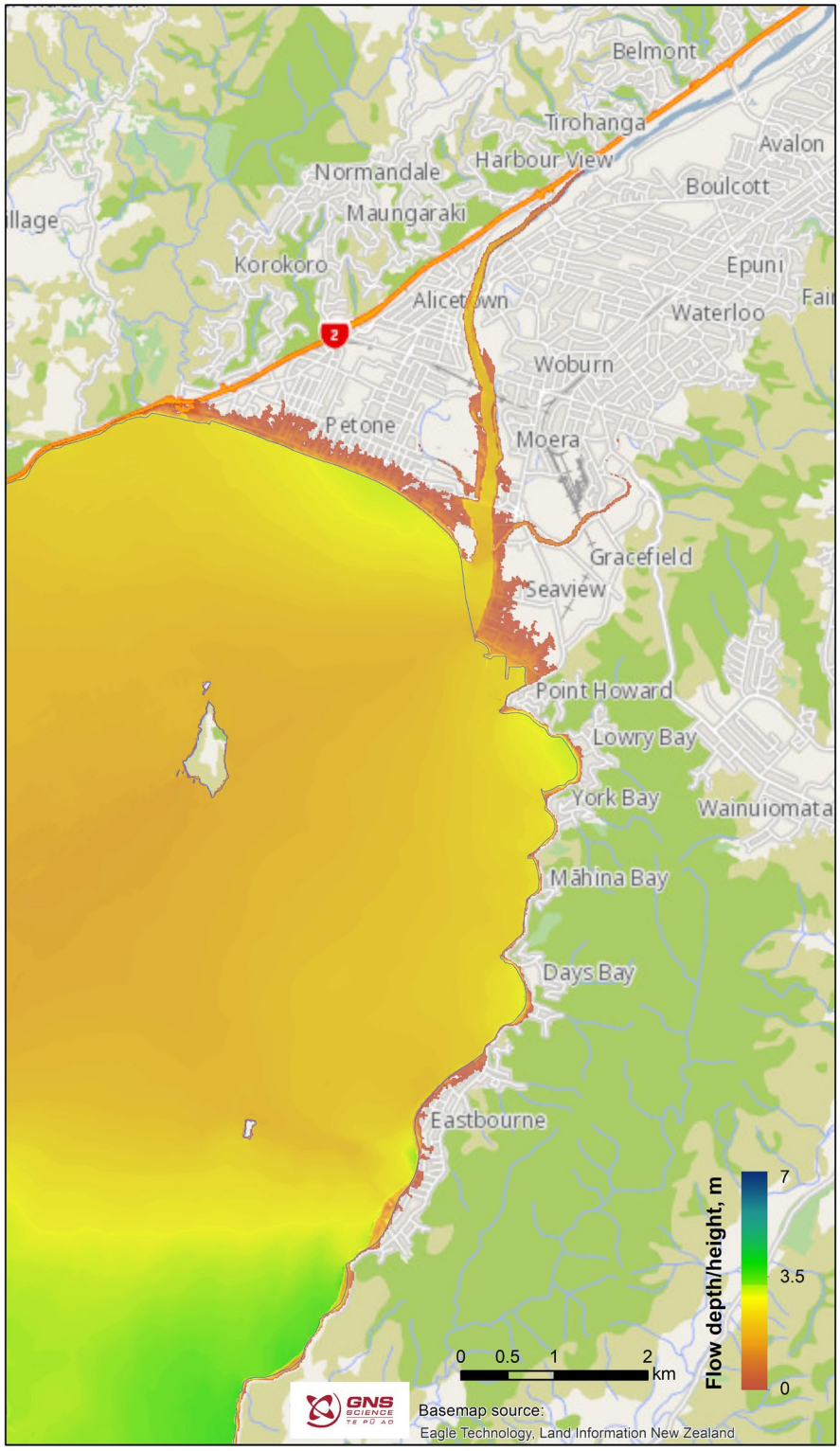

Figure 4.5 Probabilistic tsunami inundation map for Lower Hutt showing the median flow depths onshore and offshore tsunami heights with a 1-in-1000 years chance of being exceeded per annum at current MHWS. Onshore values refer to flow depths, while offshore values refer to maximum tsunami heights.

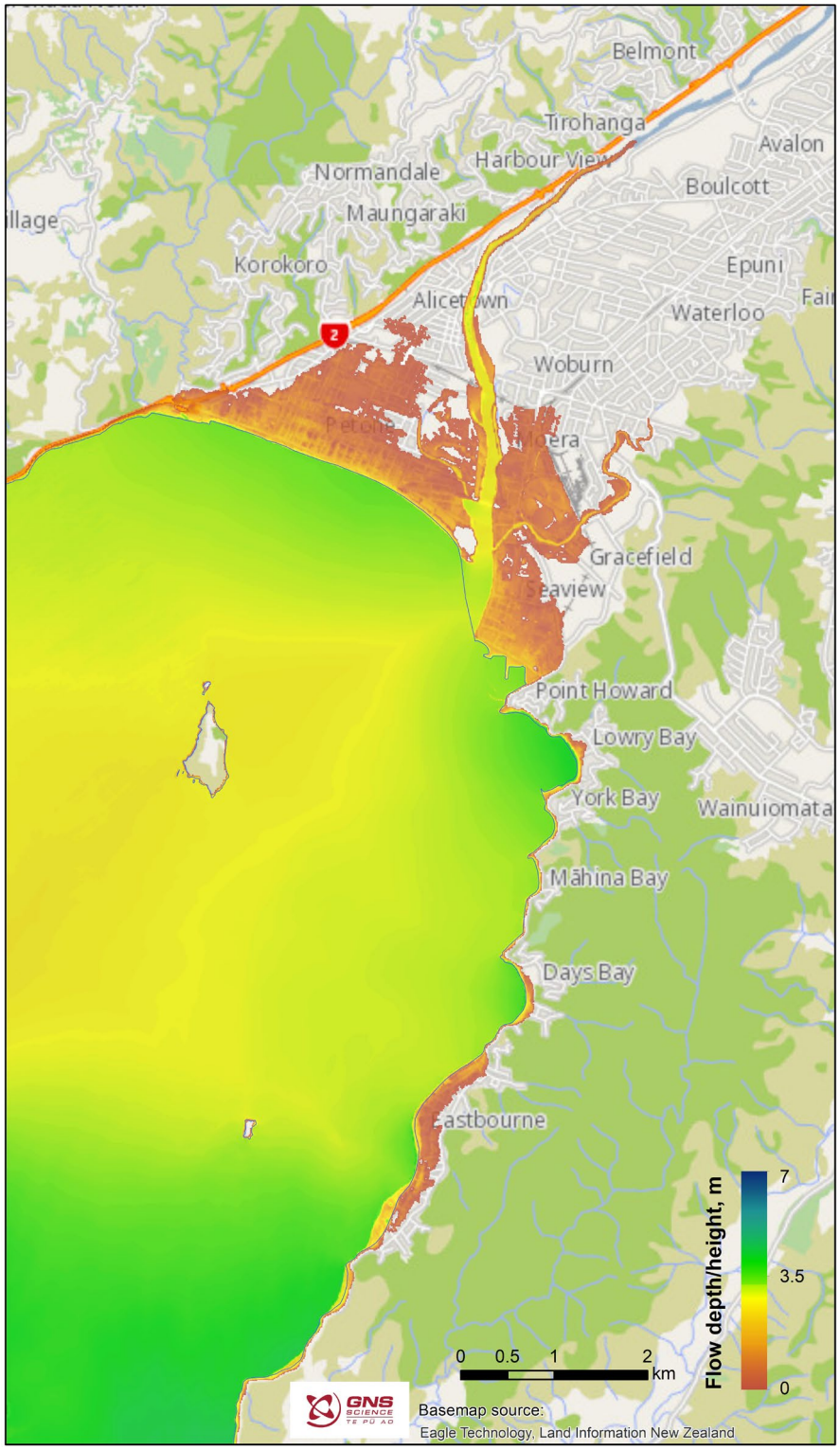

Figure 4.6 Probabilistic tsunami inundation map for Lower Hutt showing the median flow depths onshore and offshore tsunami heights with a 1-in-1000 years chance of being exceeded per annum at current MHWS **plus 1.0 m of sea-level rise**. Onshore values refer to flow depths, while offshore values refer to maximum tsunami heights.

5.0 DISCUSSION

The simulations carry several unknowns that could lead to over- or under-estimation of the actual amount of inundation observed for each scenario and thus in the combined hazard maps. These include uncertainties in modelled surface roughness, digital elevation and bathymetric models, as well as variability of the modelled geometry of the rupture surface of the earthquake, non-uniform slip distribution, the sequence in which slip is triggered on that surface and the rake angle of individual slip patches. These effects have not been included in this study for reasons of practicality, although an allowance for some of these effects has been incorporated into the NTHM deaggregation using the idea of an 'effective magnitude' (Power 2013; Power et al., in prep).

This study uses outputs from the NTHM 2021 revision, and the uncertainties and limitations of the NTHM (see Power et al., in prep) are applicable to this study. One example of this is the 1-in-500-year hazard map, which would look somewhat different if the Hikurangi source were to be just over 50% of the hazard after re-scaling rather than just under 50% (see Table 4.1), yet this level of uncertainty in the NTHM deaggregation is to be expected.

The reader should note that changes in DEM creation, such as more detailed representation of waterfront and stop banks, etc., as well as changes in the location of the DEM boundaries, can cause differences in the results presented in this study when compared to the previous studies. It should also be noted that the hazard maps have been calculated at the median hazard value for a particular APoE. This differs from the value typically used for evacuation map design, which is more conservative (the 84% confidence level is used in order to 'err on the side of caution' for life safety purposes, rather the 50% confidence level that is used here to give an unbiased estimate of the hazard for land-use planning). The maps have also been calculated at smaller return periods than are typically used for the yellow tsunami evacuation zones (a minimal return period of 2500 years as required by MCDEM [now NEMA] guidelines). Thus, these maps could be expected to show smaller inundation extent than maps derived for evacuation zone development. We therefore recommend that these maps are only used for land-use planning rather than evacuation zone design.

Finally, improvements in the models themselves or any of the other inputs, such as the NTHM, could result in changes in the final maps over time. However, GNS Science believes that the models presented here represent the best available maps based on the current science and that are achievable within the resource and time limitations of a project such as this. Thus, they should be suitable to help HCC improve Lower Hutt's resilience to tsunami.

6.0 ACKNOWLEDGEMENTS

We would like to thank Christof Mueller and Finn Scheele for reviewing this report.

7.0 REFERENCES

Arcement GJ, Jr; Schneider VR. 1984. Guide for selecting Manning's roughness coefficients for natural channels and flood plains. McLean (VA): US Department of Transportation, Federal Highway Administration. Report FHWA-TS-84-204; [accessed 2021 Sep]. https://www.fhwa.dot.gov/BRIDGE/wsp2339.pdf

Beavan J, Wang X, Holden C, Wilson K, Power W, Prasetya G, Bevis M, Kautoke R. 2010. Near-simultaneous great earthquakes at Tongan megathrust and outer rise in September 2009. *Nature*. 466:959–963. doi:10.1038/nature09292.

Bricker JD, Gibson S, Takagi H, Imamura F. 2015. On the need for larger Manning's roughness coefficients in depth-integrated tsunami inundation models. *Coastal Engineering Journal*. 57(2):1550005-1–13. doi:10.1142/S0578563415500059.

Burbidge DR, Gusman AR, Power WL, Wang X, Lukovic B. 2021. Wellington City probabilistic tsunami hazard maps. Lower Hutt (NZ): GNS Science. 24 p. Consultancy Report 2021/91. Prepared for Wellington City Council.

Cho YS. 1995. Numerical simulations of tsunami propagation and run-up [PhD thesis]. Ithaca (NY): Cornell University. 264 p.

Fraser S. 2014. Informing the development of tsunami vertical evacuation strategies in New Zealand [PhD thesis]. Wellington (NZ): Massey University. 309 p.

Fraser SA, Power WL, Wang X, Wallace LM, Mueller C, Johnston DM. 2014. Tsunami inundation in Napier, New Zealand, due to local earthquake sources. *Natural Hazards*. 70(1):415–445. doi:10.1007/s11069-013-0820-x.

Fujima K. 2001. Long wave propagation on large roughness. In: *Proceedings of the International Tsunami Symposium 2001 (ITS 2001)*; 2001 Aug 7–10; Seattle, Washington. Seattle (WA): NOAA Pacific Marine Environmental Laboratory. p. 891–895.

Gayer G, Leschka S, Nöhren I, Larsen O, Günther H. 2010. Tsunami inundation modelling based on detailed roughness maps of densely populated areas. *Natural Hazards Earth System Sciences*. 10(8):1679–1687. doi:10.5194/nhess-10-1679-2010.

Gusman AR, Power WL, Mueller C. 2019a. Tsunami modelling for Porirua City: the methodology to inform land use planning response. Lower Hutt (NZ): GNS Science. 51 p. (GNS Science report; 2019/80).

Gusman AR, Wang X, Power WL, Lukovic B, Mueller C, Burbidge DR. 2019b. Tsunami threat level database update. Lower Hutt (NZ): GNS Science. 110 p. (GNS Science report; 2019/67).

Imamura F, Yalciner AC, Ozyurt G. 2006. Tsunami modelling manual (TUNAMI model); [updated 2006 Apr; accessed 2021 Sep]. http://www.tsunami.civil.tohoku.ac.jp/hokusai3/J/projects/manual-ver-3.1.pdf

Kaiser G, Scheele L, Kortenhaus A, Løvholt F, Römer H, Leschka S. 2011. The influence of land cover roughness on the results of high resolution tsunami inundation modeling. *Natural Hazards Earth System Sciences*. 11(9):2521–2540. doi:10.5194/nhess-11-2521-2011.

Kennedy AB, Chen Q, Kirby JT, Dalrymple RA. 2000. Boussinesq modeling of wave transformation, breaking, and runup. Part1: 1D. *Journal of Waterway, Port, Coastal, and Ocean Engineering*. 126(1):39–47. doi:10.1061/(ASCE)0733-950X(2000)126:1(39).

Li L, Switzer AD, Wang Y, Chan C-H, Qiu Q, Weiss R. 2018. A modest 0.5-m rise in sea level will double the tsunami hazard in Macau. *Science Advances*. 4(8):eaat1180. doi:10.1126/sciadv.aat1180.

Liu PLF, Woo SB, Cho YS. 1998. Computer programs for tsunami propagation and inundation. Ithaca (NY): Cornell University. Technical Report.

Liu Y, Wang X, Wu Z, He Z, Yang Q. 2018. Simulation of landslide-induced surges and analysis of impact on dam based on stability evaluation of reservoir bank slope. *Landslides*. 15(10):2031–2045. doi:10.1007/s10346-018-1001-5.

Lynett PJ. 2002. A multi-layer approach to modeling generation, propagation, and interaction of water waves [PhD thesis]. Ithaca (NY): Cornell University. 201 leaves.

Manning R. 1891. On the flow of water in open channels and pipes. *Transactions of the Institution of Civil Engineers of Ireland*. 20:161–207.

Mountjoy JJ, Wang X, Woelz S, Fitzsimons S, Howarth JD, Orpin AR, Power WL. 2019. Tsunami hazard from lacustrine mass wasting in Lake Tekapo, New Zealand. In: Lintern DG, Mosher DC, Moscardelli LG, Bobrowsky PT, Campbell C, Chaytor JD, Clague JJ, Georgiopoulou A, Lajeunesse P, Normandeau A et al., editors. *Subaqueous mass movements and their consequences: assessing geohazards, environmental implications and economic significance of subaqueous landslides*. London (GB): Geological Society of London. p. 413–426. (Geological Society special publication; 477).

Mueller C, Power W, Fraser S, Wang X. 2015a. Effects of rupture complexity on local tsunami inundation: implications for probabilistic tsunami hazard assessment by example. *Journal of Geophysical Research: Solid Earth*. 120(1):488–502. doi:10.1002/2014JB011301.

Mueller C, Power WL, Wang X. 2015b. Hydrodynamic inundation modelling and delineation of tsunami evacuation zones for Wellington Harbour. Lower Hutt (NZ): GNS Science. 30 p. Consultancy Report 2015/176. Prepared for Wellington Region Emergency Management Office; Greater Wellington Regional Office.

Mueller C, Wang X, Power WL, Lukovic B. 2019. Multiple scenario tsunami modelling for Canterbury. GNS Science. 63 p. Consultancy Report 2018/198. Prepared for Environment Canterbury.

Okada Y. 1985. Surface deformation due to shear and tensile faults in a half-space. *Bulletin of the Seismological Society of America*. 75(4):1135–1154. doi:10.1785/BSSA0750041135.

Pallentin A, Verdier AL, Mitchell JS. 2009. Beneath the waves: Wellington Harbour [chart]. Wellington (NZ): National Institute of Water & Atmospheric Research. 1 sheet. (NIWA miscellaneous chart series; 87).

Power WL, compiler. 2013. Review of tsunami hazard in New Zealand (2013 update). Lower Hutt (NZ): GNS Science. 222 p. Consultancy Report 2013/131. Prepared for Ministry of Civil Defence & Emergency Management.

Power WL, Burbidge DR, Gusman AR. In prep. The 2021 update to New Zealand's National Tsunami Hazard Model. Lower Hutt (NZ): GNS Science.

Power WL, Gusman AR, Wang X, Lukovic B, Black JA. 2019. Pilot tsunami hazard study for Scott Base in Antarctica. Lower Hutt (NZ): GNS Science. 60 p. Consultancy Report 2019/113. Prepared for Antarctica New Zealand.

Stirling M, McVerry G, Gerstenberger M, Litchfield N, Van Dissen R, Berryman K, Barnes P, Wallace L, Villamor P, Langridge R, et al. 2012. National Seismic Hazard Model for New Zealand: 2010 update. *Bulletin of the Seismological Society of America*. 102(4):1514–1542. doi:10.1785/0120110170.

Wang X. 2008. Numerical modelling of surface and internal waves over shallow and intermediate water [PhD thesis]. Ithaca (NY): Cornell University. 245 p.

Wang X, Holden C, Power W, Liu Y, Mountjoy J. 2020a. Seiche effects in Lake Tekapo, New Zealand, in an Mw8.2 Alpine Fault earthquake. *Pure and Applied Geophysics*. 177(12):5927–5942. doi:10.1007/s00024-020-02595-w.

Wang X, Liu PLF. 2006. An analysis of 2004 Sumatra earthquake fault plane mechanisms and Indian Ocean tsunami. *Journal of Hydraulic Research*. 44(2):147–154. doi:10.1080/00221686.2006.9521671.

Wang X, Liu PLF. 2007. Numerical simulations of the 2004 Indian Ocean tsunamis – coastal effects. *Journal of Earthquake and Tsunami*. 1(3):273–297. doi:10.1142/S179343110700016X.

Wang X, Lukovic B, Power WL, Mueller C. 2017a. High-resolution inundation modelling with explicit buildings: a case study of Wellington CBD. Lower Hutt (NZ): GNS Science. 27 p. (GNS Science report; 2017/13).

Wang X, Power WL. 2011. COMCOT: a tsunami generation, propagation and run-up model. Lower Hutt (NZ): GNS Science. 121 p. (GNS Science report; 2011/43).

Wang X, Power WL, Lukovic B, Mueller C. 2017b. Effect of explicitly representing buildings on tsunami inundation: a pilot study of Wellington CBD. In: *Next generation of low damage and resilient structures: New Zealand Society for Earthquake Engineering Annual Conference*; 27–29 April 2017; Wellington (NZ). New Zealand Society for Earthquake Engineering. Paper O3C.3.

Wang X, Power WL, Mueller C, Lukovic B. 2020b. Tsunami modelling for proposed cross-harbour pipeline project. Lower Hutt (NZ): GNS Science. 41 p. Consultancy Report 2020/07. Prepared for Wellington Water Limited.

Wang X, Prasetya G, Power WL, Lukovic B, Brackley HL, Berryman KR. 2009. Gisborne District Council tsunami inundation study. Lower Hutt (NZ): GNS Science. 117 p. Consultancy Report 2009/233. Prepared for Gisborne District Council.

Wijetunge JJ, Wang X, Liu PLF. 2008. Indian Ocean tsunami on 26 December 2004: numerical modeling of inundation in three cities on the south coast of Sri Lanka. *Journal of Earthquake and Tsunami*. 2(2):133–155. doi:10.1142/S1793431108000293.

www.gns.cri.nz

Principal Location

1 Fairway Drive, Avalon
Lower Hutt 5010
PO Box 30368
Lower Hutt 5040
New Zealand
T +64-4-570 1444
F +64-4-570 4600

Other Locations

Dunedin Research Centre
764 Cumberland Street
Private Bag 1930
Dunedin 9054
New Zealand
T +64-3-477 4050
F +64-3-477 5232

Wairakei Research Centre
114 Karetoto Road
Private Bag 2000
Taupo 3352
New Zealand
T +64-7-374 8211
F +64-7-374 8199

National Isotope Centre
30 Gracefield Road
PO Box 30368
Lower Hutt 5040
New Zealand
T +64-4-570 1444
F +64-4-570 4657